Molecular Neurobiology
https://doi.org/10.1007/s12035-018-1365-5

Crybb2 Mutations Consistently Affect Schizophrenia Endophenotypes in Mice

Tamara Heermann[1,2] · Lillian Garrett[1,3] · Wolfgang Wurst[1,4,5,6] · Helmut Fuchs[3] · Valerie Gailus-Durner[3] · Martin Hrabě de Angelis[3,7,8] · Jochen Graw[1] · Sabine M. Hölter[1,3]

Received: 7 August 2018 / Accepted: 25 September 2018

Abstract

As part of the βγ-superfamily, βB2-crystallin (CRYBB2) is an ocular structural protein in the lens, and mutation of the corresponding gene can cause cataracts. CRYBB2 also is expressed in non-lens tissue such as the adult mouse brain and is associated with neuropsychiatric disorders such as schizophrenia. Nevertheless, the robustness of this association as well as how CRYBB2 may contribute to disease-relevant phenotypes is unknown. To add further clarity to this issue, we performed a comprehensive analysis of behavioral and neurohistological alterations in mice with an allelic series of mutations in the C-terminal end of the *Crybb2* gene. Behavioral phenotyping of these three βB2-mutant lines *Crybb2*^{O377}, *Crybb2*^{Philly}, and *Crybb2*^{Aey2} included assessment of exploratory activity and anxiety-related behavior in the open field, sensorimotor gating measured by prepulse inhibition (PPI) of the acoustic startle reflex, cognitive performance measured by social discrimination, and spontaneous alternation in the Y-maze. In each mutant line, we also quantified the number of parvalbumin-positive (PV+) GABAergic interneurons in selected brain regions that express CRYBB2. While there were allele-specific differences in individual behaviors and affected brain areas, all three mutant lines exhibited consistent alterations in PPI that paralleled alterations in the PV+ cell number in the thalamic reticular nucleus (TRN). The direction of the PPI change mirrored that of the TRN PV+ cell number thereby suggesting a role for TRN PV+ cell number in modulating PPI. Moreover, as both altered PPI and PV+ cell number are schizophrenia-associated endophenotypes, our result implicates mutated *Crybb2* in the development of this neuropsychiatric disorder.

Keywords *Crybb2* · Schizophrenia · Parvalbumin · Prepulse inhibition (PPI) · Thalamic reticular nucleus (TRN)

Introduction

As part of the βγ-superfamily, evidence implicates βB2-crystallin (CRYBB2) protein in lens development and adult mouse brain function [1–3]. Although molecular mechanisms of *Crybb2* lens fiber and epithelial cell activity are established, work continues on mouse brain pleiotropic effects [4, 5]. As βγ-crystallins constitute a separate class of Ca^{2+}-binding

Electronic supplementary material The online version of this article (https://doi.org/10.1007/s12035-018-1365-5) contains supplementary material, which is available to authorized users.

✉ Sabine M. Hölter
hoelter@helmholtz-muenchen.de

[1] Institute of Developmental Genetics, Helmholtz Zentrum München, German Research Centre for Environmental Health, 85764 Neuherberg, Germany

[2] Present address: Max Planck Institute of Biochemistry, Munich, Germany

[3] German Mouse Clinic, Institute of Experimental Genetics, Helmholtz Zentrum München, German Research Centre for Environmental Health, 85764 Neuherberg, Germany

[4] Developmental Genetics, Technische Universität München-Weihenstephan, c/o Helmholtz Zentrum München, Munich, Germany

[5] German Centre of Neurodegenerative Diseases (DZNE), Site Munich, Feodor-Lynen-Str. 17, 81377 Munich, Germany

[6] Munich Cluster of Systems Neurology (SyNergy), Adolf-Butenandt-Institut, Ludwig-Maximilians-Universität München, Schillerstr.44, 80336 Munich, Germany

[7] Experimental Genetics, School of Life Science Weihenstephan, Technische Universität München, 85354 Freising, Germany

[8] German Center for Diabetes Research (DZD), Ingolstädter Landstr. 1, 85764 Neuherberg, Germany

protein (CaBP), the assumption is that CRYBB2 acts as a calcium buffer [6, 7]. Nevertheless, to add further clarity, *Crybb2* translation and protein transcription were investigated in the adult mouse brain [1, 4]. Transcripts of *Crybb2* and the encoded βB2-protein were found in several areas, e.g., in neurons of the olfactory bulb, the hippocampus, the cerebral cortex, and the cerebellum [1, 4]. More specifically, we showed that approximately 97% of the cells positive for the calcium-binding protein parvalbumin (PV+ cells) co-express CRYBB2 in the mouse brain. In addition, two further classes of GABAergic interneuron, characterized by the presence of calretinin and somatostatin, were CRYBB2 positive [4].

There are several βB2-crystallin gene mutations identified and examined extensively in patients and mouse models of autosomal-dominant congenital cataracts [1, 8–14]. We showed, however, *Crybb2* mutations also affect the rodent nervous system. A study conducted on the C-terminal amino acid insertion mutant $Crybb2^{O377}$ revealed alterations in the number of PV+ cells, in translation of input-to-output neuronal activity in the hippocampus and in prepulse inhibition (PPI) of the acoustic startle reflex in male $Crybb2^{O377}$ mice [4]. These phenotypes suggested that *Crybb2* mutations could play a role in schizophrenia development, since PPI modulation [15–19] and GABAergic interneuron dysfunction [20–22], particularly in PV+ neurons [23–25], are human schizophrenia core symptoms. Interestingly, a meta-analysis of gene expression quantitative trait loci (QTL) in five psychiatric disorders identified the human *Crybb2* gene as the most significant association ($q = 1.75 \times 10^{-38}$) with attention-deficit hyperactivity disorder, autism, bipolar disorder, major depressive disorder, and schizophrenia [26]. Apart from this, the evidence implicating *Crybb2* in human psychiatric illness, schizophrenia in particular, is still sparse.

Therefore, this study sought to examine the robustness of the evidence that *Crybb2* mutations affect schizophrenia endophenotypes in mice by systematically searching for consistent alterations across an allelic series of three different mouse *Crybb2* mutations. Our rationale was that while each allele may have individual effects, those effects that occur in several alleles represent a common denominator and are more likely to be biologically relevant and informative. In this sense, different alleles serve as independent replicates. For this purpose, we examined mice sharing mutations in the proteins C-terminal globular domain ($Crybb2^{Philly}$, $Crybb2^{Aey2}$, $Crybb2^{O377}$). As the first βB2-crystallin mutation described, the spontaneous $Crybb2^{Philly}$ comprises a 12 nucleotide in-frame deletion at position 580, leading to the loss of four amino acids from the fourth Greek key motif [10]. Located in the same four amino acid sequence segment as $Crybb2^{Philly}$, $Crybb2^{Aey2}$ animals possess a valine in exchange for a glutamine residue [12]. Accordingly, the assumption is that the amino acid exchange prohibits the formation of the fourth Greek key motif [10, 12]. $Crybb2^{O377}$ animals exhibit an adenine to thymine substitution at the end of *Crybb2* intron 5. Since the alteration of genomic DNA sequence leads to the exchange of the conserved AG splice acceptor, $Crybb2^{O377}$ transcripts constitute an alternative splice product, leading to 19 additional amino acids being incorporated into the C-terminal domain of the protein [1] (see Fig. 1 for comparison). In this study, mutant and littermate control males and females of $Crybb2^{Philly}$, $Crybb2^{Aey2}$, and $Crybb2^{O377}$ mice underwent several behavioral tests with potential relevance to symptoms of schizophrenia [27], as well as stereological estimation of PV+ cell numbers in selected brain regions. We used the open field as a novel environment to assess psychomotor agitation, spontaneous alternation in the Y-maze to evaluate working memory, social discrimination as an estimate of social withdrawal and short-term social recognition memory, and prepulse inhibition of the acoustic startle reflex as a measure of sensorimotor gating.

Methods

Mice

$Crybb2^{O377}$, $Crybb2^{Philly}$, and $Crybb2^{Aey2}$ mice were previously described by Ganguly et al. Kador et al., and Graw et al. respectively [1, 10, 12]. The sequence location of each mutation in the corresponding mouse line is depicted in Fig. 1a, b. All three *Crybb2* mutation lines were originally introduced on a different genetic background: the $Crybb2^{Philly}$ mouse developed spontaneously within a Swiss-Webster colony [10] and was later outcrossed for 8–10 generations to a C57BL/6NHsd background [28]. Heterozygous mice of this background were imported in 2006 from Delaware (USA) into the animal facilities of the Helmholtz Center Munich and outcrossed once to C57BL/6J. From the intercrosses of the heterozygotes, a homozygous line was established. The $Crybb2^{Aey2}$ mutant was derived on a C3HeB/FeJ genetic background [12], but was backcrossed and kept as a homozygous line on C57BL/6J background for more than 10 generations. The $Crybb2^{O377}$ mutant line was derived from a C3H/El background [1]; it was backcrossed and kept as a homozygous line on C57BL/6J background for more than 10 generations. For the experiments reported here, all homozygous mutant lines were crossed with wild-type C57BL/6JG mice, and the heterozygotes were intercrossed again to generate wild type and homozygous littermates. Mice were housed under specific pathogen-free conditions at the Helmholtz Center Munich. Housing of animals was in accordance with the German Law of Animal Protection. Performed tests were approved for the ethical treatment of animals by the responsible authority of the Regierung von Oberbayern (Government of Upper

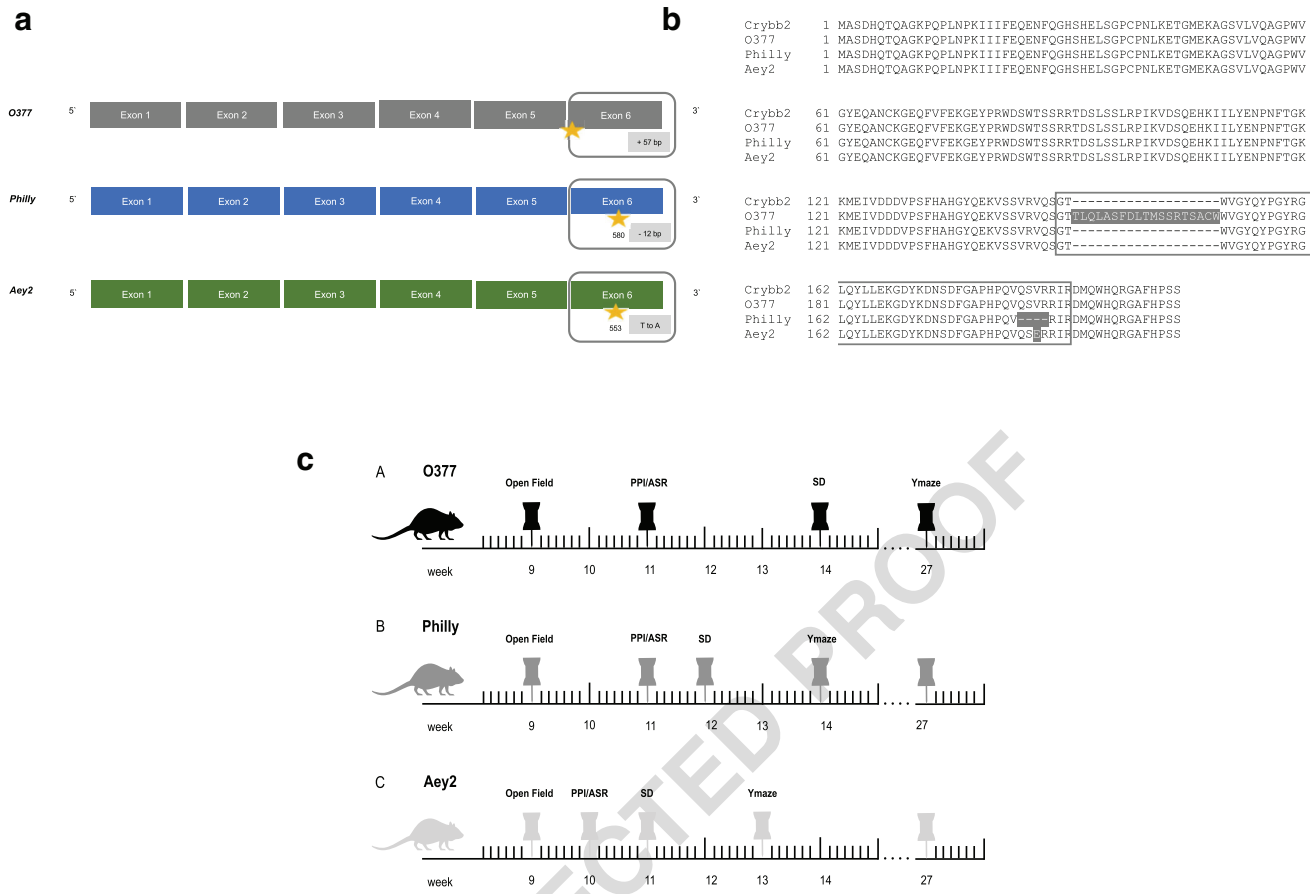

Q4 **Fig. 1** Exon structure models, amino acid sequence alignment, and conducted behavioral test battery for all examined *Crybb2* (*Crybb2*^{O377}, *Crybb2*^{Philly}, *Crybb2*^{Aey2}) mutation lines. **a** Schematic illustration of *Crybb2*^{O377}, *Crybb2*^{Philly}, and *Crybb2*^{Aey2} exon structures, resulting from mutations in the *Crybb2* allele. Approximate positions of nucleotide changes of the mRNA are indicated by a yellow star and base pair-specific sequence alterations are mentioned in the gray box. **b** Amino acid sequence alignment of *Crybb2*, *Crybb2*^{O377}, *Crybb2*^{Philly}, and *Crybb2*^{Aey2}, highlighting the location of all sequence alterations in the fourth Greek key motif, which is framed by the gray box. **c** Timeline of the conducted comprehensive behavioral test battery to assess memory, sensorimotor gating, locomotor activity, and anxiety-related behavior. For all three mutant mouse lines, we performed open field, prepulse inhibition (PPI), acoustic startle response (ASR), social discrimination (SD), and Y-maze chronologically in the specified sequence with the age in weeks shown below

Bavaria). Mice were kept in a 12/12-h dark-light cycle and provided ad libitum standard chow and water. All experiments were performed concurrently on both female and male mice homozygous for the respective mutations with wild-type littermates as controls. The number and age of animals used for each analysis is specified in Supplementary Table 1.

Behavioral Phenotyping

A cohort of each mutant mouse line was tested in a battery of behavioral assays to assess aspects of emotionality, exploratory behavior, cognition as well as sensorimotor gating and recruitment. All behavioral testing was performed in the first half of the light phase (starting 1 h after lights on), to minimize circadian rhythm effects on test performance. The battery of behavior tests was executed on mice from each mutant mouse line in the test order and age shown in Fig. 1c.

Open Field

Anxiety-related, exploratory, and locomotor activity were assessed using the open field (OF) analysis as described previously [29]. Open field analysis was initiated at 8 am and ended at 12 pm each day. The experimental setup consisted of a transparent and infra-red light permeable acrylic test arena equipped with a smooth floor and internal measurements of 45.5 × 45.5 × 39.5 cm (ActiMot, TSE, Bad Homburg, Germany). Illumination levels were set to 200 Lux in the center and approximately 150 Lux in peripheral areas. Animal movements were traced through light beam breaks (52 Hz, 28 mm apart), mouse's center of gravity was calculated according to the number of interrupted beams, and further parameters (activity settings at > 0 cm/s; rearings: minimum duration 200 ms) were automatically collected in the 20-min trial period. Data recording and analysis was performed using the ActiMot system (TSE, Bad Homburg, Germany).

Prepulse Inhibition of the Acoustic Startle Response

Acoustic startle response (ASR) and prepulse inhibition (PPI) examination were conducted using the Med Associates Inc. (St. Albans, USA) startle equipment with background noise [no stimulus (NS)] set to 65 dB. Seven trial types with ascending stimulus intensities (70, 80, 85, 90, 100, 110, and 120 dB) were performed to examine ASR. For PPI assessment, each of four different prepulse intensities (67, 69, 73, and 81 dB) preceded a 110 dB startle pulse, separated by a 50-ms inter-stimulus interval. Trial types were distributed randomly in blocks of ten and each stimulus type was assessed for ten times.

Social Discrimination

Social recognition memory of all three *Crybb2* mutant lines was assessed using the social discrimination test as described by Hölter et al. [29]. After a 2 h habituation period in a fresh cage, test animals were exposed to stimulus animals (ovariectomized 129Sv females). During the first exposure time (4 min), test and stimulus animal were allowed to roam freely. After a retention interval of 2 h, both animals were re-exposed along with a second unknown stimulus animal (4 min). The duration of investigatory behavior of the test animals towards both stimulus animals was monitored throughout the whole experiment by a trained observer. A social recognition index was calculated as the quotient of time spent investigating the unfamiliar stimulus animal and the time spent investigating both the familiar and unfamiliar ovariectomized mice.

Y-maze

To identify genotype effects on spatial working memory, spontaneous alternations were examined using the Y-maze. Consisting of three identical arms (30 × 5 × 15 cm), placed at a 120° angle from each other, all animals were tested in an opaque light gray PVC arena. Illumination in the maze center was set to 100 Lux [30]. At the beginning of each test period, the mouse was placed at the end of one arm and allowed to freely move through the maze for 5 min. Consecutive entries into all three maze arms (spontaneous alternations) and the total number of entries was scored by a trained observer. The ratio of actual (total alternations) to possible alternations (total number of triplets) multiplied by 100 was defined as spontaneous alternation performance percentage. Accordingly, percentages of alternate arm returns (AARs) and same arm returns (SARs) were calculated.

Histological Analysis

For the histological analysis of *Crybb2*^{O377}, *Crybb2*^{Philly}, and *Crybb2*^{Aey2} mice, independent cohorts of 9-week-old mice from each mouse line were utilized. For each line, 6 to 7 mice per sex and genotype were perfused. For the analysis of PV+ cells, tissues from 4 male/4 female control and homozygous mutant mice were processed and analyzed.

Tissue Processing

Adult mice from a separate cohort of the *Crybb2* mutant lines were sacrificed using carbon dioxide gas and perfused by transcardial perfusion with a solution of 4% paraformaldehyde (PFA) in 0.1 M PBS (pH = 7.4). Post fixation of brains was performed in the same fixative over night at 4 °C. Brains were then transferred to a 30% (*w*/*v*) sucrose solution and stored at 4 °C until further use. Forty-micrometer-thick coronal sections were cut using a freezing microtome (Leica SM2000R, Leica Microsystems GmbH), collected in cryoprotective solution (25% ethylene glycol and 25% glycerine in phosphate buffer) and stored at 4 °C.

Parvalbumin Immunostaining

For the immunolabeling of PV+ cells, a series of every 6th coronal 40-μm section was washed 3×, each for 10 min in 0.1 M PBS (pH 7.4) at RT. Subsequently, sections were quenched for 30 min in 1:50 30% hydrogen peroxide (0.1 M PBS, pH 7.4), washed, and then blocked with PBS-T (0.24 ml Triton-x with 100 ml 0.1 M PBS, pH 7.4), containing 10% fetal calf serum (FCS), for 1 h. Afterwards, the tissue was incubated ON in a 1:1000 dilution of the primary antibody mouse monoclonal anti-parvalbumin, PV 235 (swant®, Pierrafortscha, Switzerland) in PBS-T. Sections were once more washed, blocked (30 min), and incubated in the secondary antibody Biotin-SP (long spacer) AffiniPure Goat Anti-Mouse IgG (1:300 in PBS; Jackson ImmunoResearch Inc., West Grove, USA) for 2 h. Thereafter, an ABC protocol was utilized with DAB as chromogen [31]. A negative control, with omission of the primary antibody, revealed no positive staining.

Unbiased Stereological Cell Counting

The number of PV+ cells was estimated with unbiased design-based stereology using the Stereo Investigator software (StereoInvestigator, MBF Biosciences Inc.) on every sixth serial 40-μm coronal section and the Optical Fractionator probe [32]. The Optical Fractionator is a method where the volume fraction of the tissue is used to provide a valid estimate of a cell population number within a given region. Estimates of the total number of cells (N) are determined using the following equation:

$$N = \sum Q^{-} \times (1/ssf) \times (1/asf) \times (1/tsf)$$

The ssf is the section sampling fraction, asf is the area sampling fraction, and tsf is the thickness sampling fraction (see Schmitz and Hof (2005) for discussion of the method [33]).

The utilized equipment consisted of a Zeiss Axioplan2 microscope (Zeiss, Oberhausen, Germany) equipped with a motorized stage and a CCD color camera. Cell analysis was restricted to the thalamic reticular nucleus (TRN), the anterior cingulate cortex (ACC), the granular retrosplenial cortex (RSC) and hippocampus key structures, and the dentate gyrus (DG) area, cornu ammonis area 1 (CA1) to 3. Unbiased stereological cell counting was performed bilaterally and ROIs were delineated according to Franklin and Paxinos (dorsal − 0.94 to − 2.30 mm; ventral 2.46 to − 3.80 mm) [34]. Hippocampal subareas were traced by morphological characteristics (high neuronal densities, Bregma level − 1.34 to − 3.16 mm) and GABA immunocytochemistry was used to contour the TRN (Bregma level − 0.70 to − 1.94 mm). The boundaries of the ACC (Brodmann's area 24, Bregma level 1.18 to − 0.10 mm) and the RSC (Brodmann's area 29, Bregma level − 0.94 to − 1.94 mm) extended in a triangular shape from the anterior body—to the genus of the corpus callosum and to the dorsal part of layer I. Grid size and counting frame parameters were set to 100/100 μm. Cell count results with a coefficient of error (Gunderson, m = 1) below 10% were taken as valid. For each brain area, the following number of sections was analyzed per animal: TRN = 5, ACC = 4, RSC = 4, DG and CA1, 2, 3 = 7. For dorsal hippocampal subareas 4 sections and for ventral proportions each 3 sections were examined. Each 4 animals were analyzed per sex and genotype.

Statistical Analysis

Data processing, statistical analysis, and graph plotting were performed using GraphPad Prism (GraphPad Software, Version 6.0c). The presence of outliers was determined using Grubbs' test (a = 0.05) on all recorded data. For behavioral data sets, the Gaussian distribution was furthermore analyzed by Shapiro-Wilk. The effects of *Crybb2* mutation on the quantity of PV+ cells, open field/PPI/Y-maze/social discrimination index analysis were evaluated using two-way analysis of variance (ANOVA), followed by a post hoc test (Bonferroni). Genotype and sex were used as independent variables. Behavioral effects on the acoustic startle response were similarly examined using a two-way repeated measures (RM) ANOVA (post hoc: Bonferroni) with startle stimulus intensity (dB) as the within-subject variable and genotype as the between subject variable. For all tests, a p value < 0.05 was used as the level of significance.

Protein Structure Prediction

Protein structure prediction for CRYBB2^{O377}, CRYBB2^{Philly}, and CRYBB2^{Aey2} was performed using a template-derived hierarchical approach. FASTA format amino acid sequences of each CRYBB2 mutation were submitted without further assignment of additional restraints, secondary structure specification, or template exclusion to the I-TASSER (Iterative Threading ASSEmbly Refinement) online tool [35–37]. C-score, estimated template modeling (TM)-score, and evaluated root-mean-square deviation (RMSD) for each, in the following used models, are indicated in the caption of Fig. 3. All structure models were plotted using PyMOL 2.1.

Results

Sensorimotor Gating Phenotype in Mutants of All Three Alleles

As the final output of the nervous system, behavioral phenotyping is essential for the assessment of functional effects caused by gene mutations in the brain [38]. In the present study, the influence of mutations in the *Crybb2* gene was evaluated using a behavioral test battery that included open field (OF), prepulse inhibition (PPI), social discrimination (SD), and spontaneous alternation in the Y-maze (see Fig. 1c). As displayed in Table 1, there were no genotype effects on spontaneous forward locomotor activity in the OF (total distance traveled) in any of the three mutant lines (see Table 1 and Supplementary Table 2). The *Crybb2*^{Aey2} mutant mice did however show an enhanced vertical exploration/rearing frequency in this environment (2-way ANOVA genotype effect $F(1,43) = 14.38$, $p = 0.0005$). In terms of anxiety-related behavior, the *Crybb2*^{Philly} mutant mice also displayed decreased percentage time in the central more aversive zone of the OF arena (2-way ANOVA genotype effect $F(1,37) = 6.62$, $p = 0.0142$). There were no genotype-related differences detected in total distance traveled in the OF center in any of the three *Crybb2* mutant lines (see Table 1 and Supplementary Table 2).

To analyze the effect of *Crybb2* mutations on working memory, we examined spontaneous alternations in the Y-maze. As indicated in Table 1, no genotype-related changes were found in the percentage of spontaneous alternations or alternate arm returns in either *Crybb2*^{O377}, *Crybb2*^{Philly}, or *Crybb2*^{Aey2} mice compared to the respective littermate controls. The percentage of same arm returns was also examined in this test and shown to be decreased in the female *Crybb2*^{Aey2} mutant mice compared to controls (2-way ANOVA genotype × sex interaction effect $F(1,41) = 12.57$, $p = 0.0010$, post hoc Bonferroni's test $p = 0.0002$ female wt vs. female *Crybb2*^{Aey2} mutant mice). As a measure of activity in the Y-maze, *Crybb2*^{Aey2} animals exhibited an increased number of arm entries (2-way ANOVA genotype effect $F(1,42) = 6.525$, $p = 0.0144$). In terms of social discrimination memory, no significant alteration in recognition index was found in any of the three *Crybb2* mutation lines (see Table 1).

Although we identified several individual, allele-specific alterations in the three examined lines, only one behavioral

Journal 12035 ArtID 1336 Proof # 1 - 02/10/2018

Table 1 Results of two-way ANOVA statistical analysis of the main parameters of the conducted behavioral tests (open field, social discrimination, Y-maze) with genotype and sex as independent variables. Mean ± SEM are indicated for each experimental group. Computed *p* values are listed for genotype, sex, and interaction effects. Underlined entries highlight significant effects and asterisks indicate determined significance levels (*$p < 0.05$, **$p < 0.01$, ***$p < 0.001$). The number of animals per group and for each test is indicated in Supplementary Table 1

	Mean ± SEM				*p* value					
	Female		Male		Genotype		Sex		Interaction	
	Control	Homozygous	Control	Homozygous						
Total distance traveled [cm], open field										
Crybb2^{O377}	21,964 ± 1494	25,232 ± 2731	18,712 ± 1344	20,009 ± 1946	0.2348	ns	0.0324	*	0.6042	ns
Crybb2^{Philly}	19,804 ± 1397	18,797 ± 1807	23,139 ± 2344	22,972 ± 1344	0.7370	ns	0.0369	*	0.8100	ns
Crybb2^{Aey2}	22,455 ± 1233	25,012 ± 904	23,863 ± 941	24,296 ± 1063	0.1658	ns	0.7456	ns	0.3220	ns
Total rearing frequency [#], open field										
Crybb2^{O377}	110 ± 9.51	127 ± 6.81	111 ± 10.08	118 ± 12.27	0.2744	ns	0.6970	ns	0.6490	ns
Crybb2^{Philly}	85 ± 7.81	78 ± 8.41	119 ± 13.79	104 ± 8.41	0.2615	ns	0.0029	**	0.6969	ns
Crybb2^{Aey2}	134 ± 6.84	164 ± 7.25	138 ± 7.05	164 ± 5.48	0.0005	***	0.8415	ns	0.8450	ns
Whole arena average speed [cm/s], open field										
Crybb2^{O377}	20.4 ± 1.52	24.3 ± 2.36	17.3 ± 1.28	18.7 ± 1.89	0.1496	ns	0.0217	*	0.5034	ns
Crybb2^{Philly}	18.1 ± 1.36	17.1 ± 1.73	21.3 ± 2.32	20.5 ± 1.31	0.5977	ns	0.0570	ns	0.9688	ns
Crybb2^{Aey2}	20.7 ± 1.06	23.4 ± 0.84	21.6 ± 0.83	22.2 ± 0.98	0.0974	ns	0.8768	ns	0.2764	ns
Total time spent in the left [%], open field										
Crybb2^{O377}	16.1 ± 1.87	13.9 ± 1.61	21.8 ± 3.26	21.0 ± 3.22	0.5725	ns	0.0209	*	0.7863	ns
Crybb2^{Philly}	24.1 ± 3.09	14.9 ± 0.88	21.4 ± 5.07	17.8 ± 1.22	0.0142	*	0.9761	ns	0.2692	ns
Crybb2^{Aey2}	18.5 ± 3.18	15.2 ± 1.20	22.2 ± 1.48	19.9 ± 1.62	0.1181	ns	0.0194	*	0.7560	ns
Total distance traveled in the left [%], open field										
Crybb2^{O377}	25.3 ± 1.32	24.7 ± 1.71	27.3 ± 1.99	26.8 ± 2.22	0.7762	ns	0.2736	ns	0.9753	ns
Crybb2^{Philly}	28.1 ± 1.88	23.4 ± 1.49	26.8 ± 4.15	25.7 ± 1.19	0.1569	ns	0.8006	ns	0.3613	ns
Crybb2^{Aey2}	24.0 ± 1.46	21.5 ± 1.11	27.6 ± 1.07	16.7 ± 1.57	0.2153	ns	0.0023	**	0.5378	ns
Social Recognition Index [a.u.], social discrimination										
Crybb2^{O377}	0.57 ± 0.03 0.03218	0.61 ± 0.05	0.45 ± 0.05	0.53 ± 0.04	0.1761	ns	0.0377	*	0.6302	ns
Crybb2^{Philly}	0.29 ± 0.06	0.06 ± 0.07	0.18 ± 0.16	0.23 ± 0.09	0.3537	ns	0.7493	ns	0.1538	ns
Crybb2^{Aey2}	0.47 ± 0.03	0.49 ± 0.05	0.58 ± 0.05	0.55 ± 0.04	0.9132	ns	0.1281	ns	0.6571	ns
Number of entries [#], Y-maze										
Crybb2^{O377}	22.8 ± 2.15	23.9 ± 1.68	20.3 ± 1.66	23.0 ± 2.26	0.3529	ns	0.4050	ns	0.6926	ns
Crybb2^{Philly}	19.1 ± 2.07	16.9 ± 0.75	17.8 ± 2.20	19.2 ± 1.65	0.8088	ns	0.7813	ns	0.3248	ns
Crybb2^{Aey2}	21.3 ± 1.23	27.5 ± 1.23	24.2 ± 1.81	30.5 ± 3.39	0.0144	*	0.2375	ns	0.9806	ns
Same Arm Returns [%], Y-maze										
Crybb2^{O377}	3.9 ± 1.52	4.0 ± 1.10	2.6 ± 1.33	1.1 ± 0.71	0.5654	ns	0.1027	ns	0.5183	ns
Crybb2^{Philly}	3.2 ± 1.02	3.4 ± 1.04	2.0 ± 1.25	3.0 ± 1.29	0.6173	ns	0.5254	ns	0.7273	ns

t1.36 **Table 1** (continued)

		Mean ± SEM				*p* value					
t1.37		Female		Male		Genotype		Sex		Interaction	
t1.38		Control	Homozygous	Control	Homozygous						
t1.39	*Crybb2*^{Aey2}	7.3 ± 2.32	0.0 ± 0.00	2.7 ± 2.32	2.8 ± 0.96	0.0012	**	0.3886	ns	0.0010	***
t1.40	Alternate Arm Returns [%], Y-maze										
t1.41	*Crybb2*^{O377}	39.0 ± 3.12	35.1 ± 2.56	39.6 ± 2.54	32.5 ± 1.58	0.0530	ns	0.6707	ns	0.6096	ns
t1.42	*Crybb2*^{Philly}	40.7 ± 2.74	37.9 ± 3.52	38.6 ± 5.78	36.3 ± 2.47	0.4584	ns	0.6044	ns	0.9480	ns
t1.43	*Crybb2*^{Aey2}	30.2 ± 4.26	39.2 ± 2.46	38.0 ± 2.59	38.8 ± 2.21	0.0934	ns	0.1985	ns	0.1638	ns
t1.44	Latency [s], Y-maze										
t1.45	*Crybb2*^{O377}	12.9 ± 2.48	128. ± 2.84	6.3 ± 1.56	8.1 ± 1.11	0.7244	ns	0.0233	*	0.6932	ns
t1.46	*Crybb2*^{Philly}	6.3 ± 1.42	8.8 ± 1.14	16.0 ± 4.52	7.3 ± 0.75	0.0891	ns	0.0300	*	0.0034	**
t1.47	*Crybb2*^{Aey2}	8.1 ± 1.86	5.1 ± 0.65	4.9 ± 0.61	7.5 ± 1.03	0.7778	ns	0.6667	ns	0.0056	**
t1.48	Spontaneous alternations [%], Y-maze										
t1.49	*Crybb2*^{O377}	57.1 ± 3.77 3.77	61.0 ± 2.53	58.1 ± 2.08	61.5 ± 3.99	0.2861	ns	0.8165	ns	0.9319	ns
t1.50	*Crybb2*^{Philly}	56.1 ± 3.28	58.7 ± 3.27	59.4 ± 5.28	60.7 ± 2.07	0.8448	ns	0.1071	ns	0.3078	ns
t1.51	*Crybb2*^{Aey2}	62.5 ± 4.88	60.7 ± 4.88	59.3 ± 2.42	58.4 ± 2.05	0.6401	ns	0.3465	ns	0.8803	ns

JrnlID 12035_ArtID 1365_Proof# 1 - 02/10/2018

phenotype was consistently detectable across all: an alteration in prepulse inhibition of the acoustic startle response, which is a measure of sensorimotor gating. As displayed in Fig. 2a, measurements of global PPI revealed a genotype effect of increased PPI in both *Crybb2*^{Philly} and *Crybb2*^{O377} mice in comparison to littermate controls (2-way ANOVA genotype effect *Crybb2*^{O377} $F(1,26) = 6.019$, $p = 0.02$; *Crybb2*^{Philly} $F(1,38) = 4.343$, $p = 0.04$). In contrast, *Crybb2*^{Aey2} mutant animals were shown to exhibit significantly decreased PPI (2-way ANOVA genotype effect *Crybb2*^{Aey2} $F(1,43) = 4.820$, $p = 0.03$). This observation was specific to *prepulse inhibition* of the acoustic startle response and did not extend to the acoustic startle response itself, in which there was only an allele- and sex-specific significant genotype effect in male *Crybb2*^{O377} mice (see Supplementary Table 3).

Global Alterations in PPI Correspond to PV+ Cell Numbers in the Thalamic Reticular Nucleus in Mutants of All Three Alleles

It is known that parvalbumin deficiency affects the acoustic startle response and prepulse inhibition in mice [40]. Thus, we

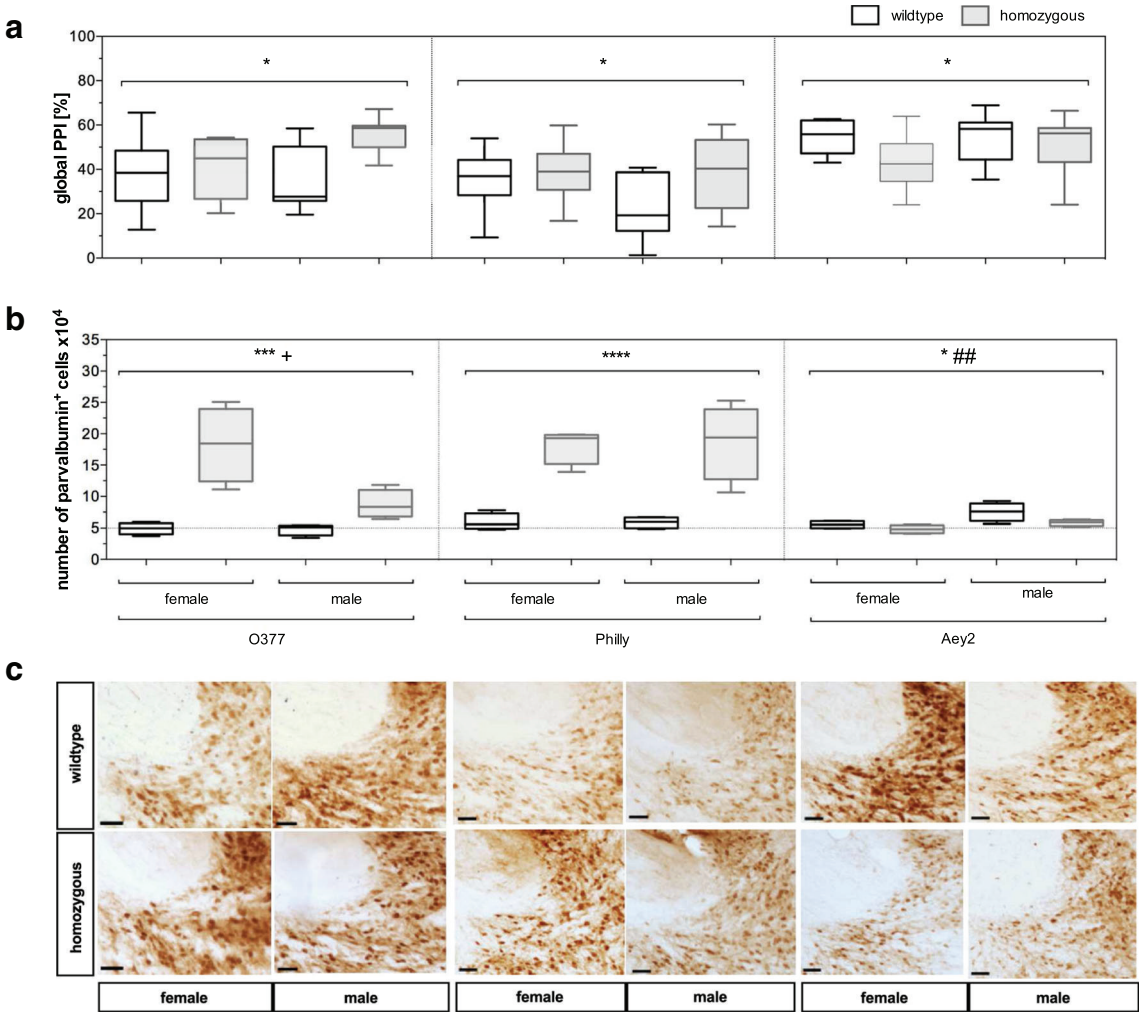

Fig. 2 Alterations in prepulse inhibition (PPI) and parvalbumin positive (PV+) cell numbers in the thalamic reticular nucleus (TRN) of *Crybb2* homozygous mutants. (A, B) Data is displayed as box-whisker plot, with indicated median and whiskers spreading between minimum and maximum values. Statistical analysis was performed by two-way analysis of variance (ANOVA), followed by a one-tailed post hoc test (Bonferroni). Genotype and sex were used as independent variables. Statistically significant effects are either displayed through asterisk (genotype), number sign (sex), or plus sign, indicating sex × genotype interaction. **a** Global evaluation of prepulse inhibition in an allelic series of mutations in the *Crybb2* gene. *Crybb2*^{O377} n[m] = 7/8, n[f] = 10/5; *Crybb2*^{Philly} n[m] = 6/13, n[f] = 11/12; *Crybb2*^{Aey2} n[m] = 12/13, n[f] = 7/15 for wild type versus homozygous animals. Asterisk indicates $p < 0.05$ genotype effect. **b** Results of unbiased stereological cell counting of TRN PV+ cells according to the optical fractionator method [39]. Five comparable Bregma levels ranging between −0.70 and −1.94 mm were analyzed per animal. *Crybb2*^{O377}, *Crybb2*^{Philly}, and *Crybb2*^{Aey2} n[m] = 4/4, n[f] = 4/4, for wild type versus homozygous animals. Corresponding statistical parameters are shown in Supplementary Table 5. Asterisk indicates $p < 0.05$; three asterisks, $p < 0.001$; four asterisks, $p < 0.0001$ genotype effect; plus sign indicates $p < 0.05$ sex × genotype interaction effect; two number signs indicate $p < 0.01$ sex effect. **c** Immunoperoxidase-stained coronal tissue sections for PV$^+$ cells. Close-up view (10×) of the superior part of the rostral thalamic reticular nucleus (Bregma level −0.82 mm). Scale bar represents 50 μm

JrnlID 12035_ArtID 1365_Proof# 1 - 02/10/2018

performed quantitative analysis of PV+ cells in the brains of all three *Crybb2* mutant and littermate control mice, to establish if alterations in PV+ neuron number accompanied the observed behavioral phenotype. The thalamic reticular nucleus (TRN) was particularly interesting in this regard, as it is rich in PV+ cells and considered a hub for corticothalamic communications. Furthermore, alterations in Ca^{2+}-binding proteins in the TRN are linked to cognitive and attentional impairments [41]. Given the density of PV+ cells, a rigorous quantitative analysis, using optical fractionator estimates, was necessary. As displayed in Fig. 2b, $Crybb2^{O377}$ and $Crybb2^{Philly}$ mice were found to possess significantly enlarged populations of PV+ cells within this region, when compared to their wild-type littermates (2-way ANOVA genotype effect $Crybb2^{O377}$ $F(1,12) = 28.15$, $p = 0.0002$; $Crybb2^{Philly}$ $F(1,12) = 53.28$, $p < 0.0001$). This effect in the $Crybb2^{O377}$ mice was driven largely by an increase in the female mutant mice compared to controls (2-way ANOVA genotype × sex interaction effect $F(1,12) = 8.33$, $p = 0.014$, *post hoc* Bonferroni's test female wt vs. mutant, $p = 0.0005$). Conversely, the $Crybb2^{Aey2}$ mice exhibited a decrease in PV+ cell numbers in the TRN (2-way ANOVA genotype effect $Crybb2^{Aey2}$ $F(1,12) = 7.34$, $p = 0.02$, for mean cell numbers see Table 2). Thus, in animals of both sexes and in all three *Crybb2* mutant lines, the alterations in global PPI corresponded to the alterations in PV+ cell numbers in the TRN: both were increased in the $Crybb2^{O377}$ and $Crybb2^{Philly}$ lines and decreased in the $Crybb2^{Aey2}$ line. While we did not correlate PPI and TRN PV+ cells (as we used two separate cohorts of mice), our results suggest a link between the number of PV+ cells in the TRN and changes in the effect direction of global PPI.

Additional Allele-Specific Alterations in PV+ Cell Numbers in Other Regions of Interest

Based on recent publications implicating anterior cingulate cortex (ACC) PV-expressing GABAergic interneurons in cognitive processes and memory integration, we performed stereological cell counting in this ROI. As displayed in Table 2, $Crybb2^{O377}$ mutant mice showed increased PV+ cells in the ACC (2-way ANOVA genotype effect $F(1,12) = 6.233$, $p = 0.03$). Independent of genotype, PV+ cell numbers were also higher in the female mice compared to males in the $Crybb2^{O377}$ line, with the opposing effect in the $Crybb2^{Philly}$ line (2-way ANOVA sex effect $Crybb2^{O377}$ $F(1,12) = 4.983$, $p = 0.045$; $Crybb2^{Philly}$ $F(1,12) = 6.321$, $p = 0.027$). Furthermore, we performed a quantitative analysis of PV+/GABAergic interneurons in the granular retrosplenial cortex (RSC). Known for its crucial role in episodic memory, the RSC extends neuronal projections to the anterior thalamic nuclei and thus the TRN [42, 43]. However, only a small increase in PV-expressing GABAergic interneurons was observed in female $Crybb2^{O377}$ mice compared to controls, with no difference in mutants harboring the other two alleles (2-way ANOVA, genotype × sex interaction effect $F(1,12) =$

Table 2 Results of two-way ANOVA analysis of the number of PV+ GABAergic interneurons in the anterior cingulate cortex (ACC), the granular retrosplenial cortex (RSC), and the thalamic reticular nucleus (TRN). Genotype and sex were used as independent variables. Underlined entries highlight significant effects and asterisks indicate determined significance levels (*$p < 0.05$, **$p < 0.01$, ***$p < 0.001$, ****$p < 0.0001$). For the analysis of the ACC and the RSC each, four sections ranging between Bregma levels 1.18 and −0.10 mm and between 1.06 and −1.94 mm were analyzed, respectively. In contrast, TRN cell numbers were determined for five sections (−0.70 and −1.94 mm). Of note, cell numbers for the ACC and the RSC were reduced by a factor of 10^3 and results for the TRN by 10^4

	Mean ± SEM				*p* value					
	Female		Male		Genotype		Sex		Interaction	
	Control	Homozygous	Control	Homozygous						
Anterior cingulate cortex										
Crybb2^{O377}	10.4 ± 1.40	17.3 ± 1.28	9.8 ± 3.73	10.8 ± 1.71	0.0281	*	0.0454	*	0.0853	ns
Crybb2^{Philly}	8.9 ± 1.03	10.7 ± 1.21	12.6 ± 0.48	12.8 ± 1.65	0.4088	ns	0.0272	*	0.4920	ns
Crybb2^{Aey2}	12.1 ± 1.25	11.5 ± 0.98	12.5 ± 1.28	15.0 ± 1.67	0.4773	ns	0.1685	ns	0.2611	ns
Granular retrosplenial cortex										
Crybb2^{O377}	7.4 ± 1.05	12.6 ± 0.71	7.8 ± 1.81	6.6 ± 0.36	0.1014	ns	0.0277	*	0.0128	*
Crybb2^{Philly}	8.5 ± 1.52	7.9 ± 0.70	9.2 ± 0.34	8.9 ± 1.28	0.6884	ns	0.4170	ns	0.8690	ns
Crybb2^{Aey2}	9.3 ± 1.28	9.6 ± 1.98	11.3 ± 1.33	10.8 ± 1.85	0.9419	ns	0.3391	ns	0.8106	ns
Thalamic reticular nucleus										
Crybb2^{O377}	4.9 ± 0.46	18.3 ± 0.45	4.8 ± 0.45	8.7 ± 1.14	0.0002	***	0.0118	*	0.0137	*
Crybb2^{Philly}	5.9 ± 0.66	18.1 ± 1.40	5.9 ± 0.45	18.7 ± 3.02	< 0.0001	****	0.8782	ns	0.8503	ns
Crybb2^{Aey2}	5.5 ± 0.30	4.8 ± 0.33	7.5 ± 0.74	5.8 ± 0.25	0.0190	*	0.0057	**	0.2933	ns

8.528, $p = 0.013$, *post hoc* Bonferroni's test $p = 0.038$, see Table 2 and Supplementary Table 5).

PV-expressing GABAergic interneurons in the hippocampus also have been associated with cognitive deficits in patients with neuropsychiatric disease [21, 22]. Thus, to elucidate further the impact of *Crybb2* mutations on this GABAergic interneuron subpopulation, we performed an optical fractionator estimate of the number of PV+ cells in this ROI. Regardless of sex, we showed a genotype-specific decline in PV+ cells of the ventral CA3 region of $Crybb2^{Aey2}$ mutant mice (2-way ANOVA genotype effect $F(1,12) = 6.06$, $p = 0.03$, see Table 3 and Supplementary Table 4), with a pattern of a decrease in the dorsal CA3 region (2-way ANOVA genotype effect $F(1,12) = 3.27$, $p = 0.096$). There were no clear differences in the other *Crybb2* mutant lines in this region. The $Crybb2^{Aey2}$ male wild-type mice showed significantly increased number of PV+ cells in the ventral CA1 region compared to the female wild-type mice (2-way ANOVA sex × genotype interaction effect $F(1,12) = 4.98$, $p = 0.045$, post hoc Bonferroni's test $p = 0.02$, Table 3). Furthermore, $Crybb2^{O377}$ mutant mice displayed increased PV+ cells in the dorsal CA2 compared to wild-type littermates (2-way ANOVA genotype effect $F(1,12) = 12.10$, $p = 0.005$). There were no effects of any of the three *Crybb2* mutations on PV+ cells in the dentate gyrus.

Discussion

So far, research on crystallins focused mainly on molecular mechanisms underlying crystallin function in the lens. However, given the ubiquitous expression of the CRYBB2 protein in the adult mouse brain and our previous findings [4], we asked if βB2 mutations consistently affect neuropsychiatric disease-related structural and functional characteristics of the brain. To this end, we used an existing allelic series of three mouse lines sharing mutations in the C-terminal domain of the CRYBB2 protein. The behavioral phenotype affected consistently across alleles was global PPI, which increased in $Crybb2^{Philly}$ and $Crybb2^{O377}$ mice and decreased in $Crybb2^{Aey2}$ animals. Substantial evidence implicates PPI alterations in schizophrenia core symptoms [17–19]. Furthermore, PPI alterations were associated with modulation of GABAergic projections from the globus pallidus [15, 16] and deficiency or inhibition of PV+ GABAergic interneurons [40, 44, 45]. Considering that 97% of PV+ cells co-express CRYBB2 in the mouse brain [4], PPI alterations in our mutant *Crybb2* lines could relate to a dysregulated PV+/GABAergic system that affects excitatory/inhibitory balance already during early development.

In light of this possible association, we scrutinized the number of PV+ GABAergic interneurons and uncovered region-specific *Crybb2* mutation-induced anomalies. Mirroring the detected alterations in global PPI, the number of PV+ interneurons increased ($Crybb2^{O377}$, $Crybb2^{Philly}$) or decreased ($Crybb2^{Aey2}$) in the TRN. While there were additional allele-specific alterations in PV+ interneuron number in other brain regions, only the alterations in the TRN occurred consistently in all three mutant lines and reflected the PPI alterations. However, given that the TRN had the highest absolute number of PV+ cells of all the brain regions assessed (see Tables 2 and 3), it might be that it is easier to detect significant differences in this nucleus. Besides the aforementioned evidence for a GABAergic role in PPI, the TRN is also part of the PPI neuronal circuitry. This was exemplified on deletion of the autism spectrum disorder associated *Ptchd1* gene in mice where PPI alterations were attenuated by reducing calcium-dependent potassium currents in the TRN [46]. Moreover, there is a link between alterations in Ca^{2+}-binding proteins of the TRN and schizophrenia-related cognitive and attentional impairments [41].

The TRN is an inhibitory shell composed of GABAergic neurons, largely PV+ interneurons. Through cortico-thalamic and thalamo-cortical connections, the TRN gates information between cortex and thalamus, pivotal to brain functions including sensory gating, attention, and sleep [43, 47–49]. Among other inputs, it receives cholinergic projections from the pedunculopontine nucleus in the brainstem, a structure integral to the PPI response [50–52]. Cholinergic TRN inhibition thereby causes disinhibition of thalamo-cortical neurons improving the relay of sensorimotor information [51, 53]. It is conceivable that interference in or enhancement of such TRN-induced gain control, through altered TRN PV+ interneuron number for example, could thus affect thalamic leakiness and the ability to filter behaviorally relevant input [54]. Given that PPI is an operational index of this ability, it may be that the *Crybb2* mouse lines are models of altered thalamic leakiness affecting PPI. While we do not yet have a direct link between altered PPI and TRN PV+ interneuron number, to our knowledge, this is the first evidence of parallel alterations in an allelic mutation series implicating specifically TRN PV+ interneuron alterations in PPI abnormalities. This concurs with evidence showing profound irregularities in TRN PV+ interneurons in schizophrenia patients [55]. In concert with the current finding, these lines of evidence point to TRN PV+ interneurons as a vulnerability site implicated in the pathophysiology of schizophrenia.

Abnormalities of the cortical (ACC, RSC) and the hippocampal (DG, CA1-3) PV+/GABAergic system were under extensive investigation in schizophrenia patients [21–25]. There are links between increased and decreased PV+ interneuron populations and the disease state [23–25,

t3.1 **Table 3** Results of two-way ANOVA analysis of the number of PV+ GABAergic interneurons in hippocampal substructures with genotype and sex as independent variables. Underlined entries highlight significant effects and asterisks indicate determined significance levels (*$p < 0.05$, **$p < 0.01$, ***$p < 0.001$, ****$p < 0.0001$). For the analysis of dorsal hippocampal subareas, 4 sections ranging between Bregma levels −1.34 and −2.18 mm and for the ventral proportion 3 sections between −2.46 and −3.16 mm were analyzed, while the entire substructure is covered through 7 sections, summarizing both dorsal and ventral proportions. Cell numbers were reduced by a factor of 10^3

		Mean ± SEM				*p* value					
		Female		Male		Genotype		Sex		Interaction	
		Control	Homozygous	Control	Homozygous						
Dentate gyrus											
Crybb2^{O377}		1.6 ± 0.37	1.5 ± 0.29	2.1 ± 0.19	2.1 ± 0.61	0.8223	ns	0.1731	ns	0.8911	ns
Crybb2^{Philly}		2.2 ± 0.18	1.7 ± 0.30	2.5 ± 0.43	2.4 ± 0.20	0.3513	ns	0.0807	ns	0.5147	ns
Crybb2^{Aey2}		2.2 ± 0.45	2.3 ± 0.40	3.7 ± 0.18	3.3 ± 0.16	0.5828	ns	0.0029	**	0.4662	ns
Dorsal dentate gyrus											
Crybb2^{O377}		1.1 ± 0.21	1.2 ± 0.25	1.4 ± 0.09	1.3 ± 0.38	0.9223	ns	0.4412	ns	0.6390	ns
Crybb2^{Philly}		1.4 ± 0.17	1.2 ± 0.16	1.5 ± 0.27	1.5 ± 0.11	0.5659	ns	0.2039	ns	0.6569	ns
Crybb2^{Aey2}		1.5 ± 0.28	1.6 ± 0.27	2.5 ± 0.16	2.1 ± 0.17	0.4828	ns	0.0064	**	0.3855	ns
Ventral dentate gyrus											
Crybb2^{O377}		0.5 ± 0.17	0.3 ± 0.04	0.7 ± 0.15	0.8 ± 0.26	0.5193	ns	0.0540	ns	0.3320	ns
Crybb2^{Philly}		0.8 ± 0.07	0.5 ± 0.15	1.0 ± 0.18	0.9 ± 0.12	0.2197	ns	0.0404	*	0.4214	ns
Crybb2^{Aey2}		0.7 ± 0.17	0.7 ± 0.13	1.2 ± 0.06	1.2 ± 0.04	0.8715	ns	0.0017	**	0.7333	ns
Cornu ammonis area 1											
Crybb2^{O377}		4.6 ± 1.14	4.6 ± 0.68	6.4 ± 0.29	7.2 ± 0.99	0.6429	ns	0.0206	*	0.6326	ns
Crybb2^{Philly}		6.8 ± 0.95	5.8 ± 1.28	12.0 ± 1.11	8.8 ± 0.62	0.0589	ns	0.0018	**	0.3130	ns
Crybb2^{Aey2}		4.9 ± 0.71	5.7 ± 0.89	9.6 ± 0.49	8.1 ± 0.20	0.5593	ns	0.0001	***	0.0829	ns
Dorsal cornu ammonis area 1											
Crybb2^{O377}		2.5 ± 4.50	3.6 ± 0.53	3.8 ± 0.56	4.2 ± 0.37	0.1608	ns	0.0732	ns	0.5458	ns
Crybb2^{Philly}		3.9 ± 0.44	3.2 ± 0.27	5.4 ± 0.36	4.8 ± 0.86	0.2295	ns	0.0119	*	0.8790	ns
Crybb2^{Aey2}		3.2 ± 0.58	3.3 ± 0.58	6.0 ± 0.19	5.4 ± 0.07	0.5176	ns	< 0.0001	****	0.4033	ns
Ventral cornu ammonis area 1											
Crybb2^{O377}		2.1 ± 0.69	1.0 ± 0.20	2.6 ± 0.39	3.0 ± 0.65	0.5305	ns	0.0321	*	0.1952	ns
Crybb2^{Philly}		3.2 ± 0.77	2.6 ± 1.02	6.5 ± 0.93	3.7 ± 0.55	0.0673	ns	0.0193	*	0.2023	ns
Crybb2^{Aey2}		1.7 ± 0.21	2.5 ± 0.41	3.6 ± 0.52	2.7 ± 0.25	0.7978	ns	0.0139	*	0.0454	*
Cornu ammonis area 2											
Crybb2^{O377}		1.3 ± 0.22	1.5 ± 0.16	2.5 ± 0.09	2.9 ± 0.54	0.3397	ns	0.0012	**	0.8499	ns
Crybb2^{Philly}		1.7 ± 0.18	1.5 ± 0.21	2.1 ± 0.15	1.9 ± 0.22	0.2870	ns	0.0444	*	0.9786	ns
Crybb2^{Aey2}		1.6 ± 0.14	1.6 ± 0.16	2.5 ± 0.20	2.3 ± 0.18	0.3970	ns	0.0008	***	0.6177	ns
Dorsal cornu ammonis area 2											
Crybb2^{O377}		0.9 ± 0.18	1.3 ± 0.12	1.0 ± 0.18	1.7 ± 0.15	0.0046	**	0.1435	ns	0.2042	ns
Crybb2^{Philly}		1.1 ± 0.09	1.0 ± 0.12	1.3 ± 0.09	1.2 ± 0.26	0.4470	ns	0.1817	ns	0.9842	ns
Crybb2^{Aey2}		1.0 ± 0.09	0.9 ± 0.10	1.8 ± 0.11	1.7 ± 0.15	0.3760	ns	< 0.0001	****	0.9219	ns
Ventral cornu ammonis area 2											
Crybb2^{O377}		0.3 ± 0.12	0.3 ± 0.1	1.6 ± 0.16	1.0 ± 0.66	0.3912	ns	0.0155	*	0.4820	ns
Crybb2^{Philly}		0.6 ± 0.13	0.5 ± 0.13	0.8 ± 0.12	0.7 ± 0.08	0.4636	ns	0.1069	ns	0.9862	ns
Crybb2^{Aey2}		0.7 ± 0.10	0.7 ± 0.07	0.6 ± 0.19	0.6 ± 0.12	0.9119	ns	0.3402	ns	0.8824	ns
Cornu ammonis area 3											
Crybb2^{O377}		7.1 ± 0.96	4.8 ± 0.37	7.6 ± 1.25	5.6 ± 2.13	0.1364	ns	0.6371	ns	0.8931	ns
Crybb2^{Philly}		6.4 ± 0.85	6.5 ± 1.23	8.9 ± 0.56	8.9 ± 0.53	0.9494	ns	0.0125	*	0.9553	ns
Crybb2^{Aey2}		9.7 ± 0.93	8.0 ± 1.26	13.5 ± 0.48	9.6 ± 0.76	0.0092	**	0.0108	*	0.2505	ns
Dorsal cornu ammonis area 3											
Crybb2^{O377}		2.6 ± 0.49	3.3 ± 0.24	2.4 ± 0.30	2.6 ± 0.58	0.3053	ns	0.2554	ns	0.6013	ns

t3.47 **Table 3** (continued)

		Mean ± SEM				*p* value					
t3.48		Female		Male		Genotype		Sex		Interaction	
t3.49		Control	Homozygous	Control	Homozygous						
t3.50	*Crybb2*^{Philly}	2.7 ± 0.30	2.6 ± 0.28	2.9 ± 0.23	2.8 ± 0.27	0.6916	ns	0.4694	ns	0.9426	ns
t3.51	*Crybb2*^{Aey2}	2.9 ± 0.32	2.7 ± 0.40	4.5 ± 0.12	3.6 ± 0.25	0.0958	ns	0.0009	***	0.3380	ns
t3.52	Ventral cornu ammonis area 3										
t3.53	*Crybb2*^{O377}	3.5 ± 0.55	2.0 ± 0.51	5.2 ± 1.48	3.0 ± 1.55	0.1338	ns	0.2585	ns	0.7599	ns
t3.54	*Crybb2*^{Philly}	3.6 ± 0.56	3.8 ± 1.14	5.9 ± 0.38	6.1 ± 0.49	0.8180	ns	0.0070	**	0.9684	ns
t3.55	*Crybb2*^{Aey2}	6.5 ± 1.02	5.4 ± 1.14	9.1 ± 0.49	6.0 ± 0.61	0.0300	*	0.0856	ns	0.2830	ns

56]. Stereological analysis of the ACC revealed an increase in PV+ expression, which was significant in *Crybb2*^{O377} mutants, particularly in female mutants, as seen before [23]. Furthermore, we were able to confirm our previous finding in male *Crybb2*^{O377} mice [4] that *Crybb2* mutations affect parvalbumin expression in *cornu ammonis* (CA) hippocampal substructures (see Table 3). In spite of the individual differences, the CA region was affected in all lines [56]. The existence of direct and indirect connections between all the investigated regions of interest in which we found alterations in *Crybb2* mutants [43, 47] suggests a PV+/GABAergic neuronal circuitry effect that may develop during early and postnatal development [1, 4]. The most consistent difference across the allelic series occurred in the TRN may be due to the relatively large proportion of highly active fast-spiking

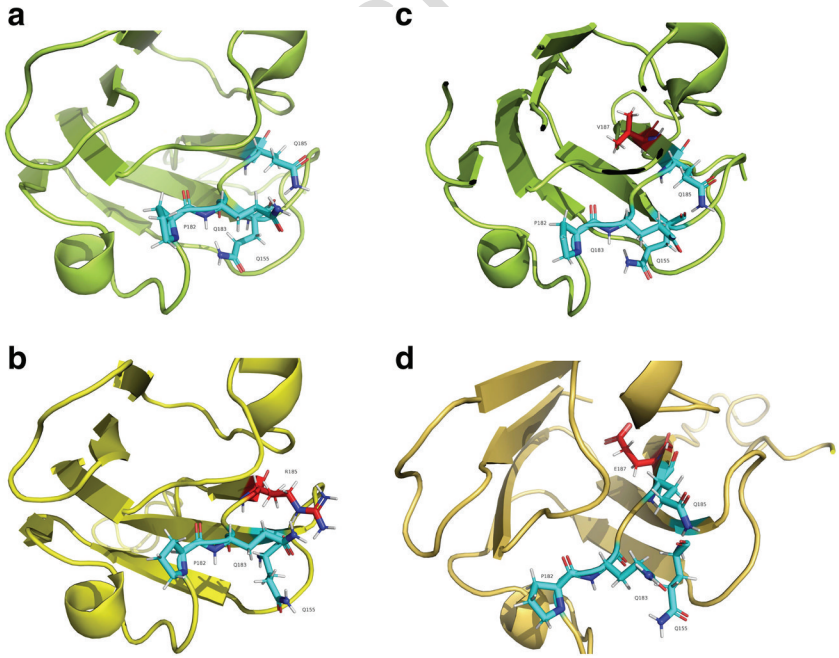

Fig. 3 Calcium complexation sites of CRYBB2 wild type, CRYBB2^{Philly}, and CRYBB2^{Aey2}. Tertiary structure models displaying the Ca^{2+} complexation motif of the C-terminal domain of CRYBB2. According to the revelations of Jobby et al., calcium complexing residues Q155, P182, Q183, and Q185 were highlighted in light blue [6]. **a** Displays a section of the model structure of the wild-type CRYBB2 protein, harboring a glutamine on position 185. In contrast, deletion of amino acids Δ185–188 in CRYBB2^{Philly} (**b**) leads to the exchange of a glutamine with an arginine on position Q185R (highlighted in red). **c** Shows a close-up of the wild-type CRYBB2 protein which possesses a valine residue on position 187 (highlighted in red). In contrast, CRYBB2^{Aey2} (**d**) displays a substitution of V187 with glutamic acid (marked in red), thus introducing a negatively charged carboxylic acid group that might enable preferable Ca^{2+} complexation. All exemplary structures were predicted using I-TASSER and models were plotted using PyMOL 2.1. CRYBB2^{Philly}: C-score = − 0.01, TM-score = 0.71 ± 0.11, and RMSD = 5.4 ± 3.4 Å. CRYBB2^{Aey2}: C-score = − 0.52, TM-score = 0.65 ± 0.13, and RMSD = 6.5 ± 3.9 Å. CRYBB2: C-score = − 0.08, TM-score = 0.70 ± 0.12, and RMSD = 5.6 ± 3.5 Å

PV+ interneurons in this region. This renders these cells particularly susceptible to challenges such as oxidative stress and possibly *Crybb2* mutation effects [55].

Of note, we did not observe consistent sex differences in *Crybb2* mutation effects, only individual ones as mentioned above which so far are of unclear relevance. But we did find sex differences in the number of PV+ cells independent of the genotype, with male mice having higher numbers of PV+ cells in several hippocampal substructures than females (see Table 3). At least for the dorsal hippocampus, this seems to be in line with a previous report that demonstrates higher levels of parvalbumin protein expression in male than in female C57BL/6 mice in the dorsal, but not in the ventral hippocampus [57]. However, in Long Evans rats recently, a higher parvalbumin protein level was reported in the dentate gyrus of females during proestrus compared to males [58]. The discrepancies might be due to species or methodological differences between the studies. Overall, the information available in the literature about sex differences in PV+ cell number or protein levels in different brain regions is selective, and still sparse. For example, sex differences have been reported in parvalbumin density in the guinea pig amygdala [59], and in the dependence of parvalbumin expression in the hippocampus on gonadal hormones during adolescent development in mice [57]. There are also several findings indicating sex differences in the effects of different kinds of physical or psychological stressors experienced during pre- or postnatal development on PV+ cells in different brain regions [60–62]. Taken together, the study of sex differences in neurodevelopmental disorders like schizophrenia is complex and requires a broader, more systematic investigation.

How could a *Crybb2* mutation alter PV+ interneuron number? A potential explanation may be CRYBB2 protein structural changes altering Ca^{2+} buffering ability that necessitates compensatory parvalbumin modifications (see Fig. 3 and the following references for more details). The CRYBB2 Ca^{2+}-binding site comprises the fourth β-strand of every Greek key motif (loops 1 and 2) [6, 7], disruption of which could alter protein-protein interactions or promote βγ-protein self-aggregation [63–65]. Using tertiary structure prediction software, we expect that disruption of one β-sheet in the Greek key motif of $CRYBB2^{O377}$ C-terminal domain would lead to aggregation and thus loss of function. This is due to an additional 19-residue loop affecting inter-domain connections of the two-domain structure [1]. On the other hand, both $CRYBB2^{Philly}$ (Δ185–188) and $CRYBB2^{Aey2}$ (V187E) will likely alter Ca^{2+} binding as they both show residue changes in or near the calcium complexation site (see Fig. 3). In the case of the former, deletion of Δ185–188 leads to the loss of one of five required sites for Ca^{2+} complexation as glutamine exchanges with arginine (Q185R). In the latter, substitution of V187 with glutamic acid introduces a negatively charged carboxylic acid group that might stabilize the negative charge required for Ca^{2+} complexation. Based on this theoretical evidence, we hypothesize that parvalbumin is upregulated (k_d 51.4 ± 2.0 nM) in $Crybb2^{O377}$ and $Crybb2^{Philly}$ interneurons to compensate the loss of Ca^{2+} buffering ability due to protein aggregation or altered Ca^{2+} ion complexation [6, 7, 66]. Conversely, parvalbumin may be downregulated as $CRYBB2^{AEY2}$ may show higher affinity Ca^{2+} binding.

Conclusion

In summary, studying an allelic series, we were able to identify consistent alterations in behavior and in the adult mouse brain associated with C-terminal mutations of the βB2-crystallin protein. Although each of the three investigated *Crybb2* mutation lines represents a different type of mutation, they all exhibit altered sensorimotor gating with parallel alterations in TRN PV+/GABAergic interneuron number. These findings suggest that, in addition to the already established neuronal circuitry, PV+/GABAergic interneurons of the TRN also contribute to the modulation of global PPI. Furthermore, changes in PV+ interneurons and in PPI are schizophrenia-associated endophenotypes. Thus, our findings together with the previously mentioned recent QTL meta-analysis in humans suggest that alterations in the function of CRYBB2 might contribute to the development of neuropsychiatric disorders.

Acknowledgements The authors thank Jan Einicke and Bettina Sperling as well as Erika Bürkle and Monika Stadler for expert technical assistance.

Authors' Contributions TH made contributions to conceptualization, methodology, formal analysis, writing (original draft), and visualization. LG made contributions to conceptualization, methodology, formal analysis, supervision, and writing (original draft). JG made contributions to conceptualization, resources, and writing (review and editing). VGD, HF, and MHdA contributed to conceptualization, methodology, and supervision of experiments at the German Mouse Clinic. WW and SMH contributed to conceptualization, resources, supervision, formal analysis, writing (original draft), and funding acquisition.

Funding This work has been funded by the German Federal Ministry of Education and Research to the GMC (Infrafrontier grant 01KX1012), to the German Center for Diabetes Research (DZD e.V.), the German Federal Ministry of Education and Research (BMBF) through the Integrated Network MitoPD (Mitochondrial endophenotypes of Morbus Parkinson), under the auspices of the e:Med Programme (grant 031A430E) as well as by the DFG grant 'DJ-1 Linked Neurodegeneration Pathways in New Mouse Models of Parkinson's Disease' (WU 164/5-1) to WW.

Compliance with Ethical Standards

Ethics Approval and Consent to Participate This animal work was approved ethically by the Regierung von Oberbayern in Germany.

Competing Interests None.

Abbreviations ACC, anterior cingulate cortex; ASR, acoustic startle response; CA1-3, cornu ammonis area 1–3; βB2-crystallin, Crybb2; DAPI, 4,6-diamidino-2-phenylindol; DG, dentate gyrus; OF, open field; PV+, parvalbumin-positive; PPI, prepulse inhibition; RSC, granular retrosplenial cortex; SD, social discrimination; TRN, thalamic reticular nucleus; QTL, quantitative trait loci

References

1. Ganguly K, Favor J, Neuhauser-Klaus A, Sandulache R, Puk O, Beckers J, Horsch M, Schadler S et al (2008) Novel allele of crybb2 in the mouse and its expression in the brain. Invest Ophthalmol Vis Sci 49(4):1533–1541. https://doi.org/10.1167/iovs.07-0788
2. Magabo KS, Horwitz J, Piatigorsky J, Kantorow M (2000) Expression of βB(2)-crystallin mRNA and protein in retina, brain, and testis. Invest Ophthalmol Vis Sci 41(10):3056–3060
3. Andley UP (2007) Crystallins in the eye: function and pathology. Prog Retin Eye Res 26(1):78–98. https://doi.org/10.1016/j.preteyeres.2006.10.003
4. Sun M, Holter SM, Stepan J, Garrett L, Genius J, Kremmer E, Hrabe de Angelis M, Wurst W et al (2013) Crybb2 coding for βB2-crystallin affects sensorimotor gating and hippocampal function. Mamm Genome 24(9–10):333–348. https://doi.org/10.1007/s00335-013-9478-7
5. Graw J (2009) Genetics of crystallins: cataract and beyond. Exp Eye Res 88(2):173–189. https://doi.org/10.1016/j.exer.2008.10.011
6. Jobby MK, Sharma Y (2007) Calcium-binding to lens βB2- and βA3-crystallins suggests that all β-crystallins are calcium-binding proteins. FEBS J 274(16):4135–4147. https://doi.org/10.1111/j.1742-4658.2007.05941.x
7. Srivastava SS, Mishra A, Krishnan B, Sharma Y (2014) Ca2+-binding motif of βγ-crystallins. J Biol Chem 289(16):10958–10966. https://doi.org/10.1074/jbc.O113.539569
8. Zhou Y, Zhai Y, Huang L, Gong B, Li J, Hao F, Wu Z, Shi Y et al (2016) A novel CRYBB2 Stopgain mutation causing congenital autosomal dominant cataract in a Chinese family. Am J Ophthalmol 2016:4353957. https://doi.org/10.1155/2016/4353957
9. Weisschuh N, Aisenbrey S, Wissinger B, Riess A (2012) Identification of a novel CRYBB2 missense mutation causing congenital autosomal dominant cataract. Mol Vis 18:174–180
10. Kador PF, Fukui HN, Fukushi S, Jernigan HM Jr, Kinoshita JH (1980) Philly mouse: a new model of hereditary cataract. Exp Eye Res 30(1):59–68
11. Bateman JB, von-Bischhoffshaunsen FR, Richter L, Flodman P, Burch D, Spence MA (2007) Gene conversion mutation in crystallin, βB2 (CRYBB2) in a Chilean family with autosomal dominant cataract. Ophthalmology 114(3):425–432. https://doi.org/10.1016/j.ophtha.2006.09.013
12. Graw J, Loster J, Soewarto D, Fuchs H, Reis A, Wolf E, Balling R, Hrabe de Angelis M (2001) Aey2, a new mutation in the βB2-crystallin-encoding gene of the mouse. Invest Ophthalmol Vis Sci 42(7):1574–1580
13. Pauli S, Soker T, Klopp N, Illig T, Engel W, Graw J (2007) Mutation analysis in a German family identified a new cataract-causing allele in the CRYBB2 gene. Mol Vis 13:962–967
14. Santhiya ST, Kumar GS, Sudhakar P, Gupta N, Klopp N, Illig T, Soker T, Groth M et al (2010) Molecular analysis of cataract families in India: new mutations in the CRYBB2 and GJA3 genes and rare polymorphisms. Mol Vis 16:1837–1847
15. Geyer MA, Krebs-Thomson K, Braff DL, Swerdlow NR (2001) Pharmacological studies of prepulse inhibition models of sensorimotor gating deficits in schizophrenia: a decade in review. Psychopharmacology 156(2–3):117–154
16. Swerdlow NR, Braff DL, Taaid N, Geyer MA (1994) Assessing the validity of an animal model of deficient sensorimotor gating in schizophrenic patients. Arch Gen Psychiatry 51(2):139–154
17. Kumari V, Soni W, Mathew VM, Sharma T (2000) Prepulse inhibition of the startle response in men with schizophrenia: effects of age of onset of illness, symptoms, and medication. Arch Gen Psychiatry 57(6):609–614
18. Mena A, Ruiz-Salas JC, Puentes A, Dorado I, Ruiz-Veguilla M, De la Casa LG (2016) Reduced prepulse inhibition as a biomarker of schizophrenia. Front Behav Neurosci 10:202. https://doi.org/10.3389/fnbeh.2016.00202
19. Hammer TB, Oranje B, Fagerlund B, Bro H, Glenthøj BY (2011) Stability of prepulse inhibition and habituation of the startle reflex in schizophrenia: a 6-year follow-up study of initially antipsychotic-naive, first-episode schizophrenia patients. Int J Neuropsychopharmacol 14(7):913–925. https://doi.org/10.1017/S1461145711000034
20. Nakazawa K, Zsiros V, Jiang Z, Nakao K, Kolata S, Zhang S, Belforte JE (2012) GABAergic interneuron origin of schizophrenia pathophysiology. Neuropharmacol 62(3):1574–1583. https://doi.org/10.1016/j.neuropharm.2011.01.022
21. Heckers S, Konradi C (2010) Hippocampal pathology in schizophrenia. Curr Top Behav Neurosci 4:529–553
22. Konradi C, Yang CK, Zimmerman EI, Lohmann KM, Gresch P, Pantazopoulos H, Berretta S, Heckers S (2011) Hippocampal interneurons are abnormal in schizophrenia. Schizophr Res 131(1–3):165–173. https://doi.org/10.1016/j.schres.2011.06.007
23. Kalus P, Senitz D, Beckmann H (1997) Altered distribution of parvalbumin-immunoreactive local circuit neurons in the anterior cingulate cortex of schizophrenic patients. Psychiatry Res 75(1):49–59
24. Borkowska M, Millar JK, Price DJ (2016) Altered disrupted-in-schizophrenia-1 function affects the development of cortical parvalbumin interneurons by an indirect mechanism. PLoS One 11(5):e0156082. https://doi.org/10.1371/journal.pone.0156082
25. Cotter D, Landau S, Beasley C, Stevenson R, Chana G, MacMillan L, Everall I (2002) The density and spatial distribution of GABAergic neurons, labelled using calcium binding proteins, in the anterior cingulate cortex in major depressive disorder, bipolar disorder, and schizophrenia. Biol Psychiatry 51(5):377–386
26. Kim Y, Xia K, Tao R, Giusti-Rodriguez P, Vladimirov V, van den Oord E, Sullivan PF (2014) A meta-analysis of gene expression quantitative trait loci in brain. Transl Psychiatry 4:e459. https://doi.org/10.1038/tp.2014.96
27. Powell CM, Miyakawa T (2006) Schizophrenia-relevant behavioral testing in rodent models: a uniquely human disorder? Biol Psychiatry 59(12):1198–1207. https://doi.org/10.1016/j.biopsych.2006.05.008
28. DuPrey KM, Robinson KM, Wang Y, Taube JR, Duncan MK (2007) Subfertility in mice harboring a mutation in βB2-crystallin. Mol Vis 13:366–373
29. Holter SM, Garrett L, Einicke J, Sperling B, Dirscherl P, Zimprich A, Fuchs H, Gailus-Durner V et al (2015) Assessing cognition in mice. Curr Protoc Mouse Biol 5(4):331–358. https://doi.org/10.1002/9780470942390.mo150068
30. Wall PM, Blanchard RJ, Yang M, Blanchard DC (2003) Infralimbic D2 receptor influences on anxiety-like behavior and active

memory/attention in CD-1 mice. Prog Neuro-Psychopharmacol Biol Psychiatry 27(3):395–410. https://doi.org/10.1016/S0278-5846(02)00356-1

31. Garrett L, Zhang J, Zimprich A, Niedermeier KM, Fuchs H, Gailus-Durner V, Hrabě de Angelis M, Vogt Weisenhorn D et al (2015) Conditional reduction of adult born doublecortin-positive neurons reversibly impairs selective behaviors. Front Behav Neurosci 9: 302. https://doi.org/10.3389/fnbeh.2015.00302
32. West MJ, Slomianka L, Gundersen HJ (1991) Unbiased stereological estimation of the total number of neurons in the subdivisions of the rat hippocampus using the optical fractionator. Anat Rec 231(4): 482–497. https://doi.org/10.1002/ar.1092310411
33. Schmitz C, Hof PR (2005) Design-based stereology in neuroscience. Neuroscience 130(4):813–831. https://doi.org/10.1016/j.neuroscience.2004.08.050
34. Franklin K, Paxinos G (1997) The mouse brain in stereotaxic coordinates. Academic Press
35. Roy A, Kucukural A, Zhang Y (2010) I-TASSER: a unified platform for automated protein structure and function prediction. Nat Protoc 5(4):725–738. https://doi.org/10.1038/nprot.2010.5
36. Yang J, Yan R, Roy A, Xu D, Poisson J, Zhang Y (2015) The I-TASSER suite: protein structure and function prediction. Nat Methods 12(1):7–8. https://doi.org/10.1038/nmeth.3213
37. Zhang Y (2008) I-TASSER server for protein 3D structure prediction. BMC Bioinformatics 9:40. https://doi.org/10.1186/1471-2105-9-40
38. Crawley JN (2008) Behavioral phenotyping strategies for mutant mice. Neuron 57(6):809–818. https://doi.org/10.1016/j.neuron.2008.03.001
39. Beauquis J, Roig P, Homo-Delarche F, De Nicola A, Saravia F (2006) Reduced hippocampal neurogenesis and number of hilar neurones in streptozotocin-induced diabetic mice: reversion by antidepressant treatment. Eur J Neurosci 23(6):1539–1546. https://doi.org/10.1111/j.1460-9568.2006.04691.x
40. Popelář J, Rybalko N, Burianová J, Schwaller B, Syka J (2013) The effect of parvalbumin deficiency on the acoustic startle response and prepulse inhibition in mice. Neurosci Lett 553:216–220. https://doi.org/10.1016/j.neulet.2013.08.042
41. Ferrarelli F, Tononi G (2011) The thalamic reticular nucleus and schizophrenia. Schizophr Bull 37(2):306–315. https://doi.org/10.1093/schbul/sbq142
42. Vann SD, Aggleton JP, Maguire EA (2009) What does the retrosplenial cortex do? Nat Rev Neurosci 10(11):792–802
43. Wright NF, Erichsen JT, Vann SD, O'Mara S, Aggleton JP (2010) Parallel but separate inputs from limbic cortices to the mammillary bodies and anterior thalamic nuclei in the rat. J Comp Neurol 518(12):2334–2354. https://doi.org/10.1002/cne.22336
44. Brown JA, Ramikie TS, Schmidt MJ, Baldi R, Garbett K, Everheart MG, Warren LE, Gellert L et al (2015) Inhibition of parvalbumin-expressing interneurons results in complex behavioral changes. Mol Psychiatry 20(12):1499–1507. https://doi.org/10.1038/mp.2014.192
45. Leppä E, Linden A-M, Vekovischeva OY, Swinny JD, Rantanen V, Toppila E, Höger H, Sieghart W et al (2011) Removal of GABA(A) receptor γ2 subunits from parvalbumin neurons causes wide-ranging behavioral alterations. PLoS One 6(9):e24159. https://doi.org/10.1371/journal.pone.0024159
46. Wells MF, Wimmer RD, Schmitt LI, Feng G, Halassa MM (2016) Thalamic reticular impairment underlies attention deficit in Ptchd1(Y/−) mice. Nature 532(7597):58–63. https://doi.org/10.1038/nature17427
47. Maren S, Holt WG (2004) Hippocampus and Pavlovian fear conditioning in rats: muscimol infusions into the ventral, but not dorsal, hippocampus impair the acquisition of conditional freezing to an auditory conditional stimulus. Behav Neurosci 118(1):97–110. https://doi.org/10.1037/0735-7044.118.1.97
48. Hartings JA, Temereanca S, Simons DJ (2003) State-dependent processing of sensory stimuli by thalamic reticular neurons. J Neurosci 23(12):5264–5271
49. McAlonan K, Cavanaugh J, Wurtz RH (2006) Attentional modulation of thalamic reticular neurons. J Neurosci 26(16):4444–4450. https://doi.org/10.1523/JNEUROSCI.5602-05.2006
50. Koch M, Kungel M, Herbert H (1993) Cholinergic neurons in the pedunculopontine tegmental nucleus are involved in the mediation of prepulse inhibition of the acoustic startle response in the rat. Exp Brain Res 97(1):71–82
51. Beierlein M (2014) Synaptic mechanisms underlying cholinergic control of thalamic reticular nucleus neurons. J Physiol 592(19): 4137–4145. https://doi.org/10.1113/jphysiol.2014.277376
52. Sokhadze G, Campbell PW, Guido W (2018) Postnatal development of cholinergic input to the thalamic reticular nucleus of the mouse. Eur J Neurosci. https://doi.org/10.1111/ejn.13942
53. Harris KD, Thiele A (2011) Cortical state and attention. Nat Rev Neurosci 12(9):509–523. https://doi.org/10.1038/nrn3084
54. Schmitt LI, Halassa MM (2017) Interrogating the mouse thalamus to correct human neurodevelopmental disorders. Mol Psychiatry 22(2):183–191. https://doi.org/10.1038/mp.2016.183
55. Steullet P, Cabungcal JH, Bukhari SA, Ardelt MI, Pantazopoulos H, Hamati F, Salt TE, Cuenod M et al (2017) The thalamic reticular nucleus in schizophrenia and bipolar disorder: role of parvalbumin-expressing neuron networks and oxidative stress. Mol Psychiatry. https://doi.org/10.1038/mp.2017.230
56. Schmalbach B, Lepsveridze E, Djogo N, Papashvili G, Kuang F, Leshchyns'ka I, Sytnyk V, Nikonenko AG et al (2015) Age-dependent loss of parvalbumin-expressing hippocampal interneurons in mice deficient in CHL1, a mental retardation and schizophrenia susceptibility gene. J Neurochem 135(4):830–844. https://doi.org/10.1111/jnc.13284
57. Wu YC, Du X, van den Buuse M, Hill RA (2014) Sex differences in the adolescent developmental trajectory of parvalbumin interneurons in the hippocampus: a role for estradiol. Psychoneuroendocrinology 45:167–178. https://doi.org/10.1016/j.psyneuen.2014.03.016
58. Ravenelle R, Berman AK, La J, Mason B, Asumadu E, Yelleswarapu C, Donaldson ST (2018) Sex matters: females in proestrus show greater diazepam anxiolysis and brain-derived neurotrophin factor- and parvalbumin-positive neurons than males. Eur J Neurosci 47(8):994–1002. https://doi.org/10.1111/ejn.13870
59. Rowniak M, Bogus-Nowakowska K, Robak A (2015) The densities of calbindin and parvalbumin, but not calretinin neurons, are sexually dimorphic in the amygdala of the guinea pig. Brain Res 1604:84–97. https://doi.org/10.1016/j.brainres.2015.01.048
60. Wischhof L, Irrsack E, Osorio C, Koch M (2015) Prenatal LPS-exposure–a neurodevelopmental rat model of schizophrenia–differentially affects cognitive functions, myelination and parvalbumin expression in male and female offspring. Prog Neuro-Psychopharmacol Biol Psychiatry 57: 17–30. https://doi.org/10.1016/j.pnpbp.2014.10.004
61. Holland FH, Ganguly P, Potter DN, Chartoff EH, Brenhouse HC (2014) Early life stress disrupts social behavior and prefrontal cortex parvalbumin interneurons at an earlier time-point in females than in males. Neurosci Lett 566:131–136. https://doi.org/10.1016/j.neulet.2014.02.023
62. Leussis MP, Freund N, Brenhouse HC, Thompson BS, Andersen SL (2012) Depressive-like behavior in adolescents after maternal separation: sex differences, controllability, and GABA. Dev Neurosci 34(2–3):210–217. https://doi.org/10.1159/000339162

63. Vendra VPR, Agarwal G, Chandani S, Talla V, Srinivasan N, Balasubramanian D (2013) Structural integrity of the Greek key motif in βγ-crystallins is vital for central eye lens transparency. PLoS One 8(8):e70336. https://doi.org/10.1371/journal.pone.0070336

64. Moreau KL, King JA (2012) Protein misfolding and aggregation in cataract disease and prospects for prevention. Trends Mol Med 18(5):273–282. https://doi.org/10.1016/j.molmed.2012.03.005

65. Liu BF, Liang JJ (2006) Domain interaction sites of human lens βB2-crystallin. J Biol Chem 281(5):2624–2630. https://doi.org/10.1074/jbc.M509017200

66. Lee SH, Schwaller B, Neher E (2000) Kinetics of Ca2+ binding to parvalbumin in bovine chromaffin cells: implications for [Ca2+] transients of neuronal dendrites. J Physiol 525(Pt 2):419–432